Photophysics and Photochemistry of an Asymmetrically Substituted Diazene: A Suitable Cage Effect Probe

Pablo A. Hoijemberg,[†] Jochen Zerbs,[‡,⊥] Christian Reichardt,[§] Dirk Schwarzer,[§] Carlos A. Chesta,[||] Jörg Schroeder,[‡] and Pedro F. Aramendía*[,†]

INQUIMAE and Departamento de Química Inorgánica, Analítica y Química Física, Facultad de Ciencias Exactas y Naturales, Universidad de Buenos Aires, Pabellón 2, Ciudad Universitaria, 1428 Buenos Aires, Argentina, Institut für Physikalische Chemie, Georg-August Universität, Göttingen, Germany, Department of Spectroscopy and Photochemical Kinetics, Max-Planck-Institute of Biophysical Chemistry, 37070 Göttingen, Germany, and Departamento de Química, Facultad de Ciencias Exactas, Fisicoquímicas y Naturales, Universidad Nacional de Río Cuarto, 5800-Río Cuarto, Argentina

Received: October 21, 2008; Revised Manuscript Received: March 23, 2009

The photophysics and photochemistry of (1-biphenyl-4-yl-1-methyl-ethyl)-*tert*-butyl diazene were thoroughly studied by laser flash photolysis from the picosecond to the microsecond time domain. The compound has favorable features as a radical photoinitiator and as a probe for cage effect studies in liquids, supercritical fluids, and compressed gases. The biphenyl moiety acts as an antenna efficiently transferring electronic energy to the dissociative ^{1}n,π^* state centered on the azo moiety. By picosecond experiments irradiating at the biphenyl- and at the azo-centered transitions, we were able to demonstrate this fact as well as determine a lifetime of 0.7 ps for the buildup of 1-biphenyl-4-yl-1-methyl-ethyl radicals (BME•). The sum of in-cage reaction rate constants of BME• radicals by combination and disproportionation is 5×10^{10} s^{-1}. The free radical quantum yield in solution is 0.21 ($\phi_{\mathrm{BME}\cdot}$) in *n*-hexane at room temperature, whereas the dissociation quantum yield approaches 50%. The symmetric ketone, 2,4-bis-biphenyl-4-yl-2,4-dimethyl-pentan-2-one, was used as a reference compound for the production and reaction of BME• radicals. Transient IR measurements show CO stretching bands of the excited $^3\pi,\pi^*$ and ^{1}n,π^* states but no dissociation up to 0.5 ns. A fluorescence lifetime of 1 ns for this ketone is consistent with this observation. By transient actinometry and kinetic decays in the microsecond time range, we measured $\varepsilon_{\mathrm{BME}\cdot} = (2.3 \pm 0.2) \times 10^4$ M^{-1} cm^{-1} at 325 nm and a second-order rate constant of 5.8×10^9 M^{-1}s^{-1} for the consumption of BME• radicals.

1. Introduction

The chemistry and photochemistry of azoalkanes was extensively studied by Engel[1] and Adam.[2] The prominent reactive feature of azoalkanes, by which they were extensively used as radical polymerization initiators,[3] is the loss of molecular nitrogen to yield a pair of radicals, either thermally or photochemically. The photochemical N_2 loss is a very fast reaction. Zewail,[4] demonstrated that a sequential bond scission is responsible for the loss of nitrogen and the generation of two methyl radicals in azomethane.[5] E-Z photoisomerization usually competes with photodissociation.[1,6] Some azoalkanes also photodissociate from the Z isomer.[1]

To be an optimum photoinitiator, normal azoalkanes have two drawbacks: a low absorption coefficient and a decrease in the photodissociation yield due to competitive photoisomerization. The absorption coefficient at relevant irradiation wavelengths has been increased by the addition of a chromophore not conjugated to the azo moiety. Successful intramolecular photosensitization was achieved in two anthryl-substituted azoalkanes.[7] The referenced compounds show photodissociation quantum efficiencies as high as 74% and have larger than 80% electronic energy transfer yield from the anthryl moiety to the azo group. These compounds have a *tert*-butyl group bonded to one of the N atoms of the azo moiety and a dimethyl-substituted carbon atom bonded to the other N atom and bridging to the aromatic moiety. This molecular structure hinders photoisomerization, thus helping to achieve the observed high photodissociation yields. Although very detailed and complete photochemical studies were performed under steady-state conditions, no time-resolved experiments were undertaken to observe the intramolecular energy transfer process.

Azocumene is a well-studied case.[8,9] It has 0.36 quantum yield for nitrogen loss[10] and a dissociation pathway from the trans isomer. Photoisomerization plays a minor role.[8] Picosecond transient studies show that in hexane, geminate cumyl radicals can diffuse apart one hard sphere collision diameter in 13 ps, and the estimated radical geminate combination at room temperature for this system is 14%.[9]

Several diazenes and ketones were used to evaluate cage effect in solution or constrained media.[11−16] Asymmetrically substituted compounds[17] of these classes show advantages to determine the cage factor from product distribution in steady-state photolysis. For this reason, we synthesized (1-biphenyl-4-yl-1-methyl-ethyl)-*tert*-butyl diazene, an asymmetrically substituted azoalkane with a *tert*-butyl group on one N and a chromophoric biphenyl moiety on the other. The compound shows interesting properties as a radical polymerization photoinitiator: thermal stability up to 70 °C, high free radical

* Corresponding author. Tel: xx54 11 4576 3378 ext. 222. Fax: xx54 11 4576 3341. E-mail: pedro@qi.fcen.uba.ar.
[†] Universidad de Buenos Aires.
[‡] Georg-August Universität.
[§] Max-Planck-Institute of Biophysical Chemistry.
[||] Universidad Nacional de Río Cuarto.
[⊥] Present address: Deutsche Gesellschaft für Luft- and Raumfahrt, Stuttgart, Germany.

10.1021/jp809315u CCC: $40.75
Published on Web 04/20/2009

CHART 1: Structures of the Diazene and of the Ketone

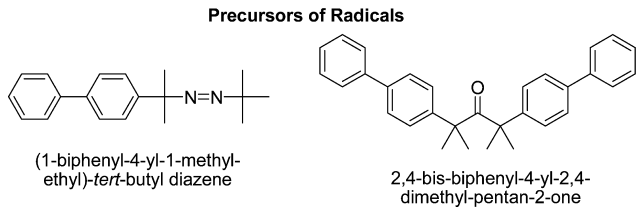

quantum yield, and high absorption coefficient at 254 nm ($2.05 \times 10^4\ M^{-1}cm^{-1}$). These features, together with a good solubility in compressed gases and in supercritical fluids, make this diazene also suitable to probe cage effect in these media.[18] The introduction of a *tert*-butyl moiety increases the efficiency of geminate combination to values greater than those for azocumene, a desired property considering the weakness of the solvent cage in supercritical fluids. In a separate work,[19] we carried out a complete product distribution and mechanistic study of the steady-state photolysis of this diazene and of a related ketone in the solid state and in solution. In the present work, we undertake a detailed picosecond and microsecond time-resolved characterization of the reactive intermediates in this system and observe the energy transfer from the biphenyl moiety to the azo group. We demonstrate, using selective excitation in the n,π^* and in the biphenyl centered π,π^* absorption bands, that intramolecular electronic energy transfer precedes the photodissociation. The formation of a π,π^* triplet excited state, centered on the biphenyl, and internal conversion are the main competitive pathways for energy dissipation. The symmetric ketone, 2,4-bis-biphenyl-4-yl-2,4-dimethyl-pentan-2-one, was used as the reference compound for the production and reaction of 1-biphenyl-4-yl-1-methyl-ethyl (BME•) radicals. Chart 1 shows the structures of the diazene and of the ketone.

2. Experimental Section

Chemicals: Synthesis of the Diazene and of the Ketone. The detailed synthesis of the diazene used in this work is described elsewhere.[19] We achieved the synthesis of the symmetric ketone 2,4-bis-biphenyl-4-yl-2,4-dimethyl-pentan-2-one[19] by using 4-biphenyl-acetic acid as a starting material in a way analogous to the procedure described by Bhandari and Ray.[20]

Microsecond Flash Photolysis. Transient absorption spectra were determined with a Spectron SL400 Nd:YAG laser generating 266 nm pulses (ca. 10 ns pulse width).[21] The laser beam was defocused to cover all of the path length (10 mm) of the analyzing beam from a 150 W Xe lamp. The measurements were performed at room temperature. The sample was contained in a rectangular quartz cell and was excited and analyzed at right angle geometry. The solution was deoxygenated by Ar bubbling. Time traces at different wavelengths in the range from 300 to 470 nm were used to reconstruct time-resolved difference spectra. The quantum yields of production of the intermediates responsible for the transient bands detected were measured by the comparative method using the naphthalene triplet as actinometer by excitation at 266 nm of N_2-bubbled solutions with matched absorbance of 0.200 in *n*-hexane.[22] Aqueous solutions of potassium dichromate were used to attenuate and vary the photolyzing laser energy.

Picosecond Flash Photolysis. Details of the experimental setup with UV−visible detection have been described elsewhere.[23] A commercial 1 kHz Ti/sapphire regenerative amplifier (Clark-MXR CPA2001) was used as the light source, delivering pulses of 150 fs duration and energy of 0.9 mJ centered at a wavelength of 773 nm. Probe pulses were generated in a TOPAS (Light Conversion) pumped by two-thirds of the laser intensity, generating wavelengths from 285 to 750 nm. For spatial filtering and divergence control, the TOPAS output was passed through a Kepler telescope and a 150 μm pinhole. We generated pump pulses of 275 nm by frequency doubling the compressed output of a two-stage NOPA (Jobin Yvon) pumped by the remaining laser energy, whereas a pump wavelength of 387 nm was obtained by generating the second harmonic of the laser fundamental.

Experiments in cyclohexane were performed in a 0.7 mm flow cell exciting at 275 nm, whereas for all of the other measurements, a stationary 1 cm quartz cell was used. The concentrations used were 0.7 mM in the flow cell and between 5 and 15 mM in the stationary cuvette. Solutions in cyclohexane (Roth, for synthesis, ≥99.5%) were bubbled with N_2.

The picosecond infrared experiments were carried out with a laser system based on a 1 kHz Ti/sapphire oscillator/regenerative amplifier system (wavelength 800 nm, pulse width 100 fs, pulse energy 700 μJ). Pump pulses at 267 nm were produced by frequency tripling part of the 800 nm light. The UV light was attenuated to energies between 0.5 and 2 μJ and used to excite 2,4-bis-biphenyl-4-yl-2,4-dimethyl-pentan-2-one dissolved in *n*-heptane. Tunable mid-infrared pulses were generated by difference frequency mixing of idler and signal from an optical parametric amplifier[24,25] pumped by 250 μJ pulse energy of the regenerative amplifier output. The IR light was split into probe and reference beams and was focused into the sample cell. At the sample, the probe pulse was superimposed on the pump beam. To avoid signal contributions arising from rotational relaxation of molecules, the relative plane of polarization of both pulses was adjusted to 54.7°. After passing the cell, both IR beams were spectrally dispersed in a grating polychromator and independently imaged on a HgCdTe detector (2 × 32 elements). The whole pump−probe setup was purged with dry nitrogen to avoid spectral and temporal distortion of the IR pulses by absorption of CO_2 and water in air. All experiments were performed in a stainless steel flow cell equipped with 1 mm thick CaF_2 windows. (The path length inside the cell was 0.6 mm.)

Absorption and Emission Spectra, Fluorescence Quantum Yield, and Lifetimes. Absorption spectra were determined using either a Hewlett-Packard 6453E diode array, a Shimadzu 160A, or a Shimadzu PC3100 spectrophotometer. Fluorescence spectra were recorded using a PTI-Quantamaster spectrofluorometer. Emission spectra were corrected by the instrument correction function. Emission of 1,1′:4′,1″-terphenyl was used as a reference for fluorescence quantum yield determination ($\phi_f = 0.82$[26]). All measurements were preformed on cyclohexane solutions (HPLC grade from Sintorgan) at room temperature. Time-resolved fluorescence decays were obtained using a PTI-TimeMaster instrument. A hydrogen pulsed lamp was used for excitation. The instrument response function was measured with the scattered light of a colloidal suspension of Ludox (50 ps per point time resolution, IRF fwhm 2.5 ns). Fluorescence decay of the ketone was recorded on a TCSPC IBH5000U system with a 282 nm, 1 MHz excitation diode laser (26 ps per point time resolution, IRF fwhm 0.8 ns, detected at 282 nm) and 2 mm GG-395 cutoff filter (Schott) in the emission.

3. Results

The photolysis of the diazene produces BME• and *tert*-butyl (*t*-Bu•) radicals as primary dissociation products with N_2 loss.

SCHEME 1[a]

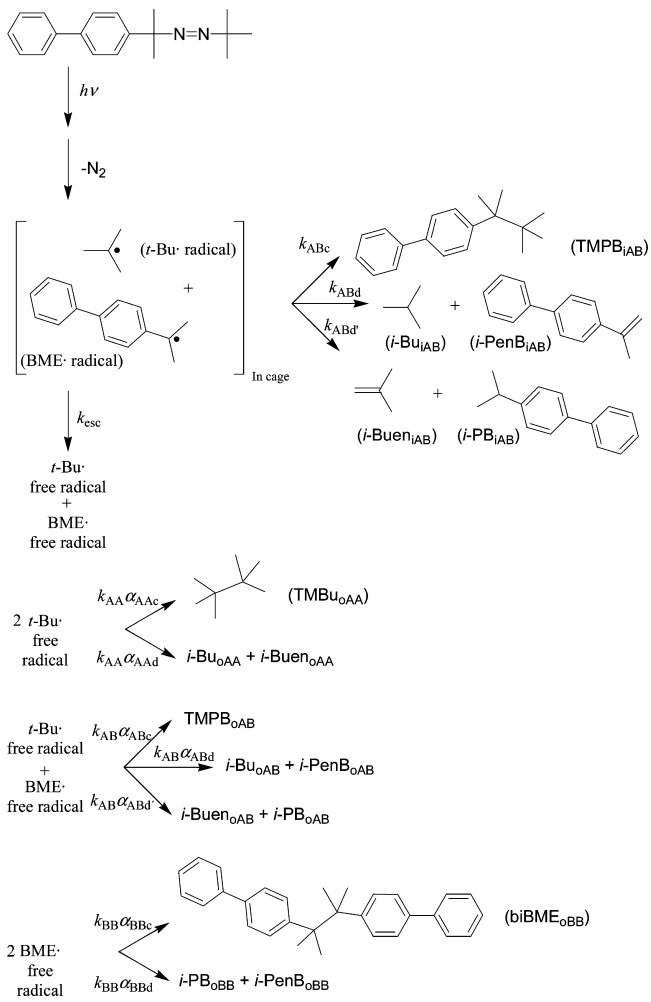

[a] Short names for compounds are given in the text above. Subscripts "i" and "o" indicate that the product was formed either "inside" the geminate cage or "outside" of it. Subscripts A or B indicate the identity of the radicals reacting to form the product, being *t*-Bu• radical A and BME• radical B. $\alpha_{ABc} = k_{ABc}/(k_{ABc} + k_{ABd} + k_{ABd'} + k_{esc})$ and corresponding expressions are valid for the other α fractions.

SCHEME 2[a]

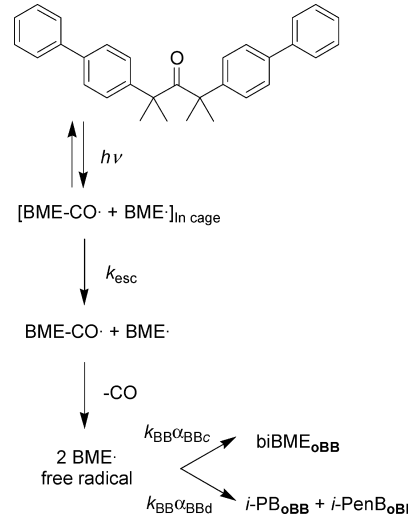

[a] Naming is given as in Scheme 1.

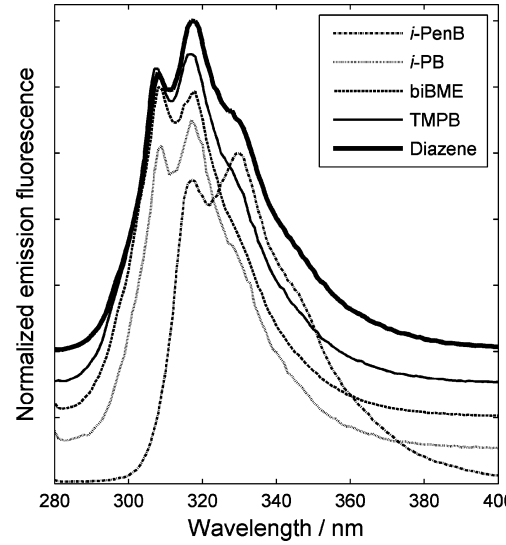

Figure 1. Maximum normalized corrected emission spectra (from bottom to top) of 4-isopropenyl-biphenyl (*i*-PenB), 4-isopropyl-biphenyl (*i*-PB), 1,1′-bis(1-biphenyl-4-yl-1-methyl-ethyl) (biBME), and 4-(1,1,2,2-tetramethyl-propyl)-biphenyl (TMPB) and of the emission developed upon diazene irradiation (diazene) at 254 nm in cyclohexane deoxygenated solutions. The spectra were shifted in the vertical direction for clarity.

However, the symmetric ketone can only yield BME• radicals after CO loss. The mechanisms in Scheme 1, for the diazene, and Scheme 2, for the ketone, account for the observed products.

Figure 1 shows the normalized emission spectra of *i*-PenB, *i*-PB, biBME, and TMPB. (See caption of Figure 1 for acronym definitions and Scheme 1 for structures.) All compounds have biphenyl-like emission spectra (with slight vibrational structure and a somewhat red-shifted spectrum for *i*-PenB). A very low fluorescence intensity was detected from the diazene when excited at 254 nm in freshly prepared solutions. This emission spectrum is excitation-wavelength-dependent. When a freshly prepared solution is excited at 280 nm, the emission displays a maximum at 335 nm and a shoulder at 350 nm, resembling the emission of *i*-PenB. After a second scan of the same solution, an emission spectrum develops that increases in intensity upon successive scans. Normalized emission spectra have practically identical shapes after a 35-fold increase in total emission intensity, using the 254 nm excitation beam of the spectrofluorometer for photolysis and excitation (Figure 1). This fact reveals buildup of fluorescent products via efficient photodissociation.

In cyclohexane solution, the fluorescence decay lifetime and quantum yield for the products of the photolysis of the diazene are: *i*-PB 4.5 ns, 0.09 ± 0.03; biBME 6.63 ns, 0.15 ± 0.03; TMPB 7.61 ns, 0.12 ± 0.03; and *i*-PenB 1.0 ns, 0.30 ± 0.03.

The ketone does not show biphenyl-like emission. Instead, its fluorescence spectrum is structureless with a maximum around 320 nm and a shoulder at 390 nm from a band extending up to 450 nm. Upon successive scans, as in the case of the diazene, because of product formation, the biphenyl-type emission starts to develop, but the emission above 380 nm shows practically no variation because of low conversion of the ketone. Consequently, the decay time of the ketone was measured in this emission range. The ketone has $\phi_f = 0.005$ with a lifetime of 1.1 ns.

Figures 2 and 3 show difference absorption spectra of the diazene and of the ketone when photolyzed at 266 nm with nanosecond laser pulses. Two bands are identified: one with a maximum at 330 nm, decaying with second-order kinetics in the microsecond time range, and a second band with a maximum

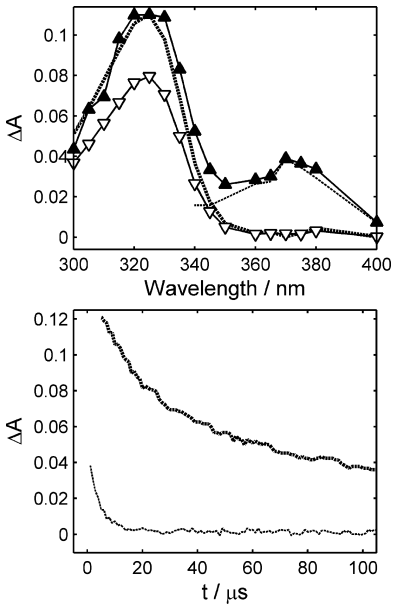

Figure 2. Top: difference absorption spectra after photolysis of a N_2-bubbled 4×10^{-5} M solution of diazene in *n*-hexane with a nanosecond laser pulse at 266 nm: ▲, 1 μs after laser pulse; ▽, 25 μs after laser pulse. The thick dashed line between 300 and 350 nm is the spectrum at 25 μs normalized to the spectrum at 1 μs. The thin dashed line between 340 and 400 nm is the difference between the spectrum at 1 μs and the thick dashed line spectrum. Bottom: decay kinetic curves at 325 (thick dashed line) and 370 nm (thin dashed line).

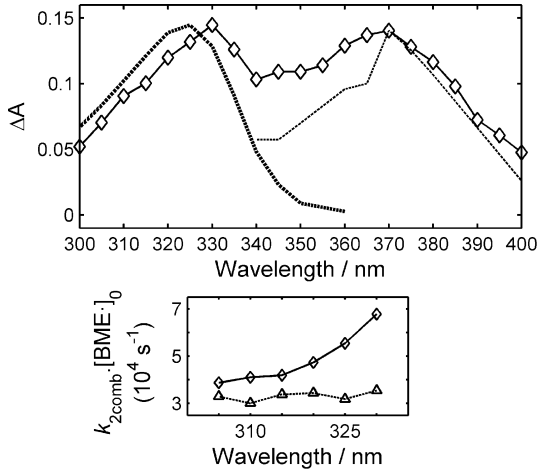

Figure 3. Top: difference absorption spectrum immediately after photolysis of a N_2-bubbled 4×10^{-5} M ketone solution in *n*-hexane with a nanosecond laser pulse at 266 nm (◊). Thick and thin dashed lines are the difference absorption spectra of the same components from Figure 2 normalized to the maximum of each band. Bottom: plot of the ratio of slope and intercept (proportional to k_{2comb}.[BME•]$_0$) of the second-order kinetic plots for the diazene (lower curve, △) and the ketone (upper curve, ◊) as a function of analyzing wavelength.

at 370 nm, decaying with a first-order decay rate constant of 2.2×10^5 s^{-1}.

The similarity of these two bands in spectroscopic and kinetic features points to two common intermediates in these systems on this time scale. We assign the band at 330 nm to the BME• radical because of its spectroscopic similarities with benzyl-type radicals and its second-order decay kinetics,[8,27] whereas the band at 370 nm corresponds to the biphenyl-centered triplet state absorption. (See below.)

The slope of the second-order kinetic plots of the differential absorbance decays (ΔA) renders the ratio between the second-order rate constant, k_{2comb}, and the absorption coefficient of the radical at the analyzing wavelength, $\varepsilon_{BME\cdot}$, as expressed by eq 1. (In the 300−340 nm range, the absorption coefficient of the ground state is negligible compared with $\varepsilon_{BME\cdot}$; see below.) In Scheme 1, $k_{2comb} = [2k_{BB} + k_{AB}](1 - f_{esc})$, and in Scheme 2, $k_{2comb} = 2k_{BB}(1 - f_{esc})$, where $f_{esc} = k_{esc}/(k_{esc} + k_{reac})$, and k_{reac} is the sum of all in-cage reactive rate constants, as illustrated in Scheme 1.[28]

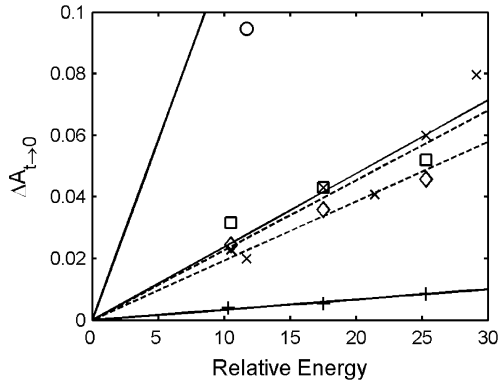

Figure 4. Extrapolated difference absorbance immediately after a nanosecond laser pulse of 266 nm as a function of pulse energy. N_2-bubbled solutions in hexane with matched absorbance of 0.200 at the excitation wavelength. Symbols and lines correspond to: naphthalene triplet monitored at 422 nm (○, black solid line); diazene monitored at 320 nm (×, gray solid line); diazene monitored at 370 nm (+, black solid line); ketone monitored at 320 nm (◊, gray dashed line); ketone monitored at 370 nm (□, black dashed line). Other experimental points for triplet naphthalene are out of scale.

$$\frac{1}{\varepsilon_{BME\cdot}.[BME\bullet]} = \frac{1}{\varepsilon_{BME\cdot}.[BME\bullet]_0} + \frac{k_{2comb}}{\varepsilon_{BME\cdot}}t \qquad (1)$$

As eq 1 shows, $\varepsilon_{BME\cdot}$ must be known to obtain the value of the second-order rate constant. Second-order kinetics plots are quite sensitive to baseline variations, absorption band overlap, and small residual absorbance at the apparent end of the decay. For this reason, we plot in the bottom of Figure 3 the value of the slope divided by the intercept of the plots, according to eq 1, as a function of wavelength for each compound. The value of this ratio in a pure second-order decay is equal to the product of k_{2comb} and the initial concentration of intermediate, that is, k_{2comb}.[BME•]$_0$. It should be constant if there is no overlap of bands and if the initial concentration of combining radicals is equal in all experiments for each compound. We assume the latter condition is fulfilled for each compound because all single wavelength curves were recorded under otherwise identical conditions and in random order. The overlap of the short-lived triplet and the BME• radical absorption leads to higher apparent values of the second-order rate constant for the ketone because of the greater triplet yield in the latter case. However, the diazene shows a practically constant value in the bottom plot of Figure 3 in the 300−340 nm range. Therefore, we will derive the values of second-order rate constants from these experiments once we calculate $\varepsilon_{BME\cdot}$. (See below.) The slope of the linearized second-order decay plot of BME• radical transient decay at 325 nm is 2.6×10^5 cm/s for the diazene.

The band at 370 nm is assigned to the biphenyl-centered $^3\pi,\pi^*$ because of its spectroscopic and kinetic similarities with the pure biphenyl triplet excited state.[22]

The results of the relative quantum yield of production of the intermediates responsible for these bands, using the naphthalene triplet as actinometer, are plotted in Figure 4. The ratio of slopes for any two intermediates is given by eq 2, where

subscript "ref" indicates the naphthalene triplet and "X" is any of the other unknowns.

$$\frac{(\text{slope})_X}{(\text{slope})_{ref}} = \frac{\varepsilon_X \phi_X}{\varepsilon_{ref} \phi_{ref}} \quad (2)$$

Using for the naphthalene triplet $\varepsilon = 2.45 \times 10^4\ M^{-1}\ cm^{-1}$ [29] and $\phi_{isc} = 0.75$,[30] we calculated triplet quantum yields of 0.016 and 0.11 for the diazene and the ketone, respectively, assuming for their triplets an absorption coefficient at 370 nm equal to that of the biphenyl triplet: $\varepsilon = 4.3 \times 10^4\ M^{-1}\ cm^{-1}$.[30]

The quantum efficiency for the disappearance of the diazene under steady-state photolysis conditions is $\phi_{-diazene} = 0.38 \pm 0.05$ for irradiation at 254 nm and $\phi_{-diazene} = 0.50 \pm 0.05$ for irradiation at 365 nm. This difference indicates that fast internal conversion from the $^1\pi,\pi^*$ to the ground state competes with electronic energy transfer to the dissociative $^1n,\pi^*$ state.[19] This formal internal conversion can be considered to be an intramolecular energy transfer and will be referred to as such in the following because the two chromophores are not conjugated.

Figure 4 shows that the efficiency of production of free BME· radicals in solution ($\phi_{BME\cdot,free}$) is 1.2 times greater for the diazene than for the ketone. For the diazene: $\phi_{BME\cdot,free} = f_{esc} \cdot \phi_{-diazene}$. Product distribution indicates an average of 0.44 ± 0.07 for the ratio of in-cage to total products for the diazene.[19] This value is the cage factor for the BME· and *t*.Bu· radicals, $f_{cage} = (k_{ABc} + k_{ABd} + k_{ABd'})/(k_{esc} + k_{ABc} + k_{ABd} + k_{ABd'}) = 1 - f_{esc}$. Therefore, $\phi_{BME\cdot,free} = 0.21 \pm 0.05$ for the diazene at 254 nm irradiation, and $\phi_{BME\cdot,free} = 0.17 \pm 0.05$ for the ketone.

Figure 5 (top) shows difference absorption spectra after femtosecond laser flash photolysis of the diazene in cyclohexane solution at 275 and 387 nm. These spectra are different and correspond to excitation of the diazene to the $^1\pi,\pi^*$ excited state centered on the biphenyl ring (275 nm excitation) and to the $^1n,\pi^*$ excited state centered in the azo moiety (387 nm excitation of the same system). After ca. 45 ps, the two difference absorption spectra become similar and resemble the spectrum obtained immediately after ns photolysis of the diazene (Figure 5, bottom). The absence of the absorption corresponding to the triplet at 45 ps after excitation at 387 nm indicates that the $^3\pi,\pi^*$ centered on the biphenyl originates from the $^1\pi,\pi^*$.

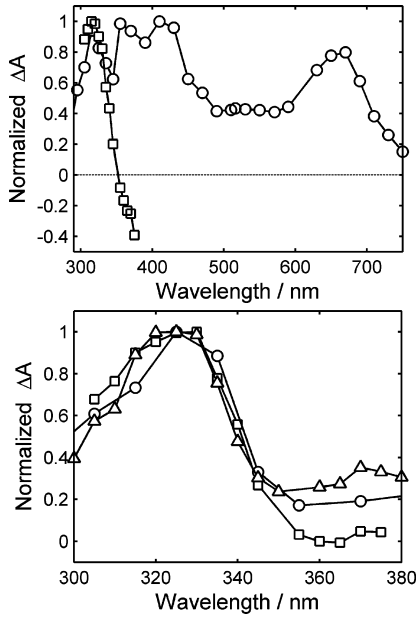

Figure 5. Top: difference absorption spectrum 0.75 ps after 200 fs laser photolysis of a N_2-bubbled diazene solution in cyclohexane at 275 (○) and 387 nm (□). Bottom: difference absorption spectrum after laser photolysis of a N_2-bubbled diazene solution in cyclohexane: ○, 45 ps after excitation at 275 nm with 200 fs pulse; □, 45 ps after excitation at 387 nm with 200 fs pulse; △, immediately after nanosecond excitation at 266 nm with ns pulse.

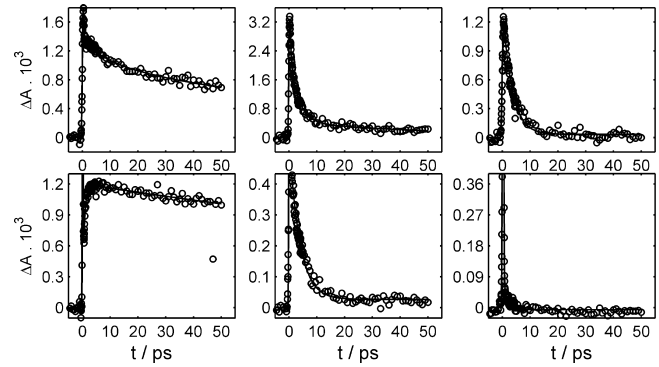

Figure 6. Transient difference absorption signals after femtosecond photolysis of a N_2-bubbled diazene solution in cyclohexane. The three upper curves pump at 275 nm, and the three lower curves pump at 387 nm. The two curves on the left were monitored at 330 nm, the two in the middle were monitored at 450 nm, and the two on the right were monitored at 670 nm.

The initial spectrum obtained after excitation at 275 nm shows two broad and very intense absorption bands (Figure 5, top). These bands, centered at 410 and 670 nm, are typical bands of the biphenyl excited singlet state.[31] The transient absorption signals recorded at these wavelengths have much smaller amplitude after 387 nm excitation. In the latter spectrum, the negative difference absorption observed above 350 nm is due to ground-state bleaching.

Figure 6 shows transient absorption traces at different excitation and monitoring wavelengths. Upon 275 nm excitation, only decaying curves are observed. The decay lifetime of ca. 3.5 ps observed at 450 and 670 nm corresponds to the decay of the biphenyl-centered $^1\pi,\pi^*$ state. Even at 387 nm, there seems to be a residual excitation of the biphenyl-centered absorption, as reflected by the small signals depicted in Figure 6 in the lower row (measured at 450 and 670 nm in the center and right traces, respectively). After 387 nm excitation, a signal buildup is detected at around 330 nm with a lifetime of 0.7 ps, corresponding to the formation of the BME· radical. The buildup of this radical is not detected upon 275 nm excitation because of the overlap with the strong absorption of the biphenyl-centered $^1\pi,\pi^*$, which has a lifetime of 3.5 ps. The BME· radical is responsible for the absorption band between 300 and 350 nm remaining after 45 ps in the samples excited at both wavelengths. The $^3\pi,\pi^*$ centered on the biphenyl is responsible for the absorption in the 350−400 nm range remaining after 45 ps. The decays registered after 387 nm excitation in the wavelength range of 350−380 nm show growing signals because of the recovery of the ground-state absorption. No recovery with a lifetime shorter than 1 ps is observed. They can be obscured by the pulse autocorrelation peak because of their expected small amplitude. Only a small buildup with 3 ps lifetime is observed corresponding to ground-state recovery from the $^1\pi,\pi^*$.

The slowest decay observed in the picosecond time window, with a lifetime of 20 ps is observed in the curves monitored at 330 nm (Figure 6) and is assigned to in-cage reactions and to transient diffusion effects in the encounter of BME· radicals.[9,32]

Photoisomerization is ruled out because no signal is observed at the expected wavelength range for the cis isomer (ca. 400

SCHEME 3: Reaction Scheme for the Diazene Showing the Events from the Different Excited States and Intramolecular Electronic Energy Transfer

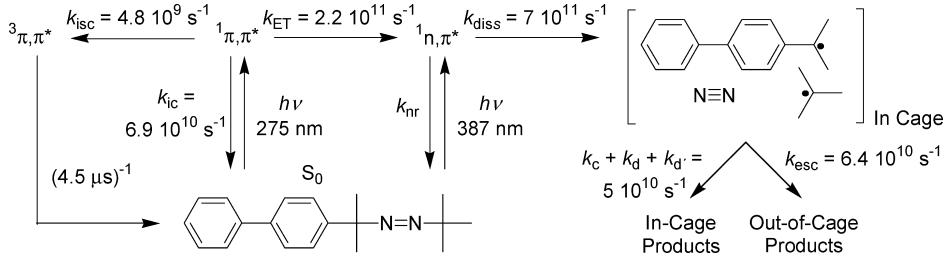

nm),[8] neither in the transient measurements nor upon low-temperature irradiation (*n*-hexane at −80 °C).

Scheme 3 summarizes the kinetics results for the diazene. It shows the reaction pathways from the different excited states including intramolecular electronic energy transfer.

Figure 7 shows the difference absorption spectrum after femtosecond laser photolysis of the ketone pumping at 275 nm. The spectrum shows two bands that appear instantaneously in this time range and vary little up to 45 ps after the pulse. There is no evidence of the absorption due to the $^1\pi,\pi^*$ state centered on the biphenyl, meaning that this state very promptly (<0.5 ps) decays to the $^1n,\pi^*$ state centered on the ketone and to the $^3\pi,\pi^*$ state centered on the biphenyl. The former is responsible for the absorption between 290−350 nm, which strongly resembles the spectrum of the diazene after 387 nm excitation. The $^3\pi,\pi^*$ state accounts for the band around 370 nm. Small variations of the absorption, taking place in the mentioned time range, are due to vibrational relaxation. The dissociation of the ketone $^1n,\pi^*$ state to the BME-CO• acyl radical and the BME• radicals takes place with ca. 1 ns lifetime, beyond the observation time of the experiment and too fast to be observed in the microsecond time range experiments.

In Figure 8, we show the fingerprint region of the measured and calculated stationary IR spectrum of the ketone together with the transient difference spectrum obtained in *n*-heptane at a time delay of 1.3 ns after excitation at 267 nm. The prominent features are the bleach of the strongest ketone band at 1685 cm^{-1} and the appearance of two new comparably strong absorption bands at 1570 and 1295 cm^{-1}. The bleach, visible at 1600 cm^{-1}, belongs to an as yet unidentified impurity. The strong 1685 cm^{-1} parent band mainly derives its intensity from the CO stretch. Accordingly, the high intensity of the two red-shifted bands at 1570 and 1295 cm^{-1} suggests dominant contributions from the CO stretch as well. Neither of these bands can be assigned to the BME-CO• radical because it is expected that the corresponding IR band is blue-shifted with respect to that of the parent compound, an expectation born out also by the calculated BME-CO• spectrum. Because the BME• radical apparently does not possess comparably strong IR absorption lines, we are led to the conclusion that the bands at 1570 and 1295 cm^{-1} have to be assigned to CO-stretch modes in electronically excited states of the ketone. Furthermore, there is clearly no absorption detected at the stretch frequency of the bare CO molecule. In view of the evidence from time-resolved electronic spectroscopy presented above, we assign them to the CO stretch in the $^1n,\pi^*$ and $^3\pi,\pi^*$ states. Because much stronger red shifts of the CO stretch have been observed between S_0 and n,π^* states than between S_0 and π,π^* states,[33−36] we assign the 1295 cm^{-1} band to the $^1n,\pi^*$ CO stretch and the 1570 cm^{-1} band to the $^3\pi,\pi^*$ CO stretch. Figure 9 depicts the time evolution of these two bands and of the bleach at 1685 cm^{-1} in the picosecond time domain. In all three cases, the band appears within the experimental time resolution of ∼0.5 ps and within experimental error limits remains constant afterward. The only time evolution we observe on the picosecond time scale is band

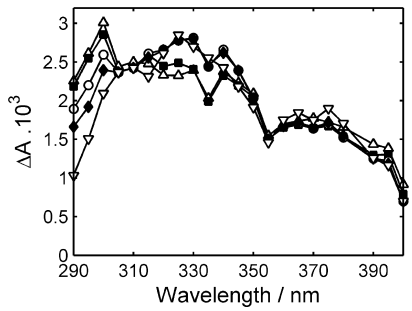

Figure 7. Difference absorption spectrum at different delays after 200 fs pulsed laser photolysis of the ketone at 275 nm in N_2-bubbled cyclohexane solution. Curves correspond to times of 0.75, 1, 5, 10, and 45 ps for △, ■, ○, ♦, and ▽, respectively.

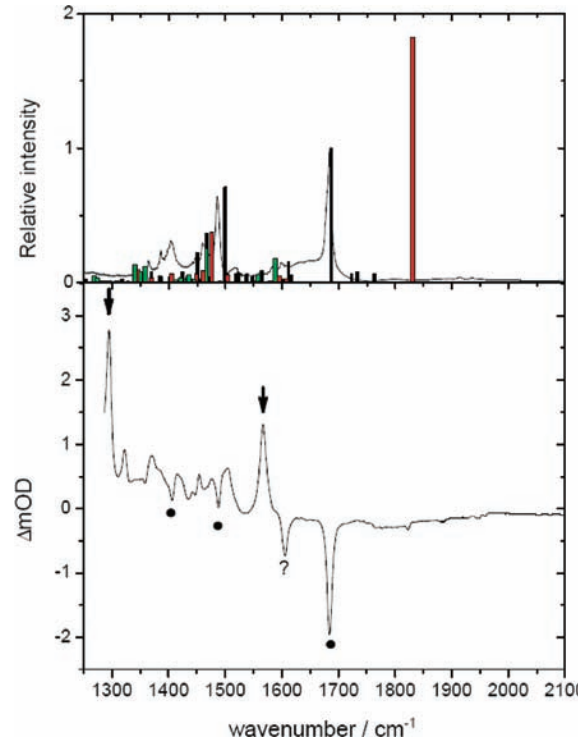

Figure 8. Top: stationary IR spectrum of the ketone together with the calculated stick spectrum of the ketone (black), the BME-CO radical (red), and the BME radical (green). Bottom: transient IR absorption spectrum at 1.3 ns time delay following excitation at 267 nm. ● denotes bleached bands of the parent compound; ↓ denotes the two main new absorption bands. The bleached band marked with ? may be due to a currently unidentified impurity.

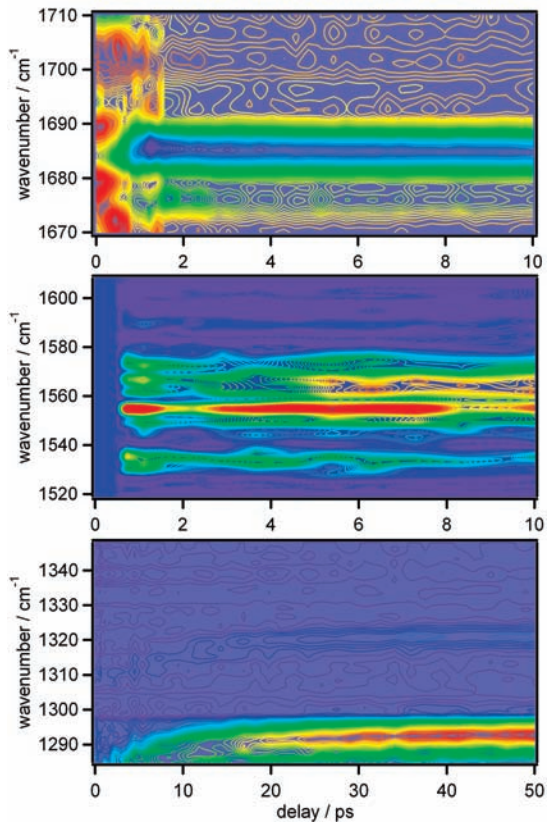

Figure 9. Time evolution of the CO stretch bands: bleach in S_0 (top), new absorption bands in $^3\pi,\pi^*$ (middle), and ^{1}n,π^* (bottom). Because different spectral regions are covered in separate measurements, time zeros do not exactly match. In the bottom diagram (note longer time scale), the band shifts into the observation window as vibrational cooling takes place on a ~10 ps time scale.

narrowing and a slight blue shift, the typical signature of vibrational cooling. In conclusion, the transient IR absorption measurements confirm that excitation of the $^1\pi,\pi^*$ transition in the ketone is followed by ultrafast population of the ^{1}n,π^* and $^3\pi,\pi^*$ states that do not decay within the time range accessible in these experiments. All of the above information on the ketone leads us to the reaction scheme in Scheme 4, where the events from the different excited states are shown.

4. Discussion

The emission recorded in freshly prepared solutions of the diazene with 280 nm excitation is equivalent to 1.5% *i*-PenB content, assuming that all emission originates from this compound, the main photolysis product in the solid state.[19] We have no evidence of emission originating from the diazene. If we consider *i*-PB (singlet state lifetime 4.5 ns, $\phi_f = 0.09$) to be a model for the emission properties of the diazene, the 3.5 ps excited-state lifetime of its biphenyl-centered $^1\pi,\pi^*$ would imply $\phi_f < 10^{-4}$, which is consistent with the observations.

The primary photochemical event is a C−N bond cleavage in the diazene. There are two possibilities for this bond scission. If we assume that nitrogen loss is fast compared with any possible reaction of the azenyl alkyl geminate radical pair,[5,37] then any of the two primary scissions will lead to the same pair of alkyl radicals and nitrogen in the reaction cage. Under this assumption, $\phi_{-diazene}$ equals the quantum yield of the primary bond cleavage. Because there is no evidence of photoisomerization, we can assume that internal conversion is the only remaining deactivation pathway. Photoisomerization is greatly hindered by the presence of the two methyl substituents in each carbon bound to the nitrogen atoms.

We cannot discern if the complete dissociation of the diazene is a concerted or a sequential process. We see only one lifetime for the formation of the BME• radical, but this can be the result of a sequential process with one lifetime falling below the time resolution of our experiments (70 fs for azomethane[4]) or a consequence of the primary dissociation of the diazene exclusively rendering BME• radical and *tert*-butyl-azenyl radical, which we do not detect.

Our results show that the dissociation of the diazene takes place from the ^{1}n,π^* state. A possible dissociation pathway through a triplet state cannot be ruled out, but it should make a minor contribution to dissociation. On one side, we do not observe any radical buildup with the $^3\pi,\pi^*$ decay lifetime in the microsecond experiments in either the diazene or the ketone (with a triplet yield similar to the dissociation yield). On the other side, it is unlikely that intersystem crossing from the ^{1}n,π^* to the ^{3}n,π^* state can compete favorably with 1.4×10^{12} s^{-1}, the decay rate constant of the ^{1}n,π^* state.

The ketone probably dissociates from the ^{3}nπ^* state and not from the $^3\pi\pi^*$ state. The microsecond measurements rule this out because we see no increase in the radical signal with 5 μs lifetime (the decay time of the $^3\pi\pi^*$ for both compounds). The ^{3}nπ^* state is not detected in the picosecond experiments because it originates upon the decay of the ^{1}nπ^* state with 1 ns lifetime. Additionally, the dissociation of the excited ketone is also expected to take place in this time range,[11] making the ^{3}nπ^* state difficult to detect.

The difference in the values of $\phi_{-diazene}$ following excitation of the $^1\pi,\pi^*$ and ^{1}n,π^* bands indicates that intramolecular electronic energy transfer between the $^1\pi,\pi^*$ and ^{1}n,π^* states is 76% efficient.

The 3.5 ps lifetime observed for the $^1\pi,\pi^*$ state of the diazene is consistent with the absence of emission from the biphenyl excited moiety, as discussed above. Therefore, the presence of the azo moiety in the diazene, with its dissociative ^{1}n,π^* state acting as a funnel for the electronic energy, is responsible for the short lifetime of the diazene's biphenyl-centered $^1\pi,\pi^*$ state compared with the *i*-PB $^1\pi,\pi^*$ excited state, and C−N bond dissociation is responsible for the extremely short excited-state lifetime of the diazene ^{1}n,π^* state. Using the lifetime of the $^1\pi,\pi^*$ and the 1.6% intersystem crossing yield for the diazene gives $k_{isc} = 4.8 \times 10^9$ s^{-1} for the intersystem crossing rate constant.

If we take into account the fact that the ^{1}n,π^* state has a lifetime of 0.7 ps and dissociates with 0.5 quantum yield, then we can calculate a value of 7×10^{11} s^{-1} for the total dissociation rate constant to yield the two possible pairs of azenyl- and carbon-centered radicals. Furthermore, considering the in-cage reaction rate of 5×10^{10} s^{-1} for the BME• radicals (20 ps lifetime) and their 56% cage escape efficiency, a value of 6.4×10^{10} s^{-1} is calculated for k_{esc}. This value compares well with the 13 ps measured by Scott for the escape of geminate cumyl radicals in hexane.[9]

Rate constants for radical addition and disproportionation (Scheme 1) can be calculated by taking into account the in-cage total BME• radical consumption rate and the appropriate product distribution from a previous work.[19] All calculated rate constants are summarized in Table 1.

If we consider the value of $\phi_{BME\cdot,free} = 0.21 \pm 0.05$ for the diazene, then $\varepsilon_{BME\cdot} = (2.3 \pm 0.2) \times 10^4$ M^{-1} cm^{-1} at 325 nm is derived from the actinometries of Figure 4 and eq 2.[38] This

SCHEME 4: Reaction Scheme for the Ketone Showing the Events from the Different Excited States

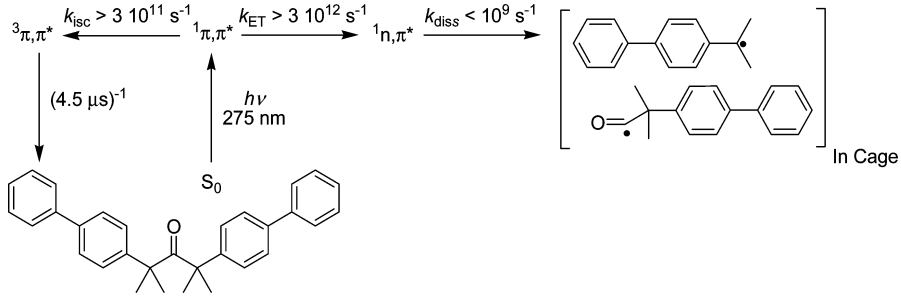

TABLE 1: Calculated Reaction Rate Constants from Schemes 1 and 3

	diazene
k_{ET}	$2.2 \times 10^{11}\ s^{-1}$
k_{isc}	$4.8 \times 10^{9}\ s^{-1}$
$1/\tau(^3\pi,\pi^*)$	$2.2 \times 10^{5}\ s^{-1}$
k_{diss}	$7 \times 10^{11}\ s^{-1}$
k_{ABc}	$3.0 \times 10^{10}\ s^{-1}$
k_{ABd}	$1.6 \times 10^{10}\ s^{-1}$
$k_{ABd'}$	$4 \times 10^{9}\ s^{-1}$
k_{esc}	$6.4 \times 10^{10}\ s^{-1}$
k_{2comb} (see text)	$5.8 \times 10^{9}\ M^{-1}\ s^{-1}$

value is twice the ε_{max} value for the benzyl radical,[39] which can be explained by the greater extension of the π orbitals in biphenyl.

The value of $\varepsilon_{BME\cdot}$ renders $k_{2comb} = 5.8\ 10^9\ M^{-1}\ s^{-1}$ for the BME· radicals. In a system where these radicals are exclusively consumed by a second-order process, $k_{2comb} = 2k_R$, where k_R is the reactive rate constant of the radicals. For the consumption of BME· radicals in the diazene, $k_{2comb} = 3k_{BB}(1 - f_{esc})$,[28] from which the values of $k_{BB} = 4.4 \times 10^9\ M^{-1}\ s^{-1}$ (eq 1) and $k_R = k_{BB}(1 - f_{esc}) = 2 \times 10^9\ M^{-1}s^{-1}$ for the total reactive rate constant of BME· radicals can be readily calculated. We can compare this latter value with the corresponding values measured for a series of benzyl radicals in cyclohexane.[40] Table 2 of this reference lists values of $2k_R$ that indicate that k_R spans the range from (1.0 to 2.3) $\times\ 10^9\ M^{-1}\ s^{-1}$ for benzyl and various substituted benzyl radicals. The expected range for these rate constants in *n*-hexane would be (3 to 7) $\times\ 10^9\ M^{-1}\ s^{-1}$ if we take into account that its viscosity is roughly three times lower than that of cyclohexane. The value obtained for k_R of BME· radicals in this work is slightly lower than the mentioned range but satisfactorily within expectations. The value of k_{BB} can be compared with the diffusion-limited rate constant multiplied by the spin statistical factor of $^1/_4$ for singlet and triplet radical reaction pairs.[41] The work by Fischer[40] estimates that k_R coincides with the diffusion-limited encounter rate constant (including the $^1/_4$ spin statistical factor) within ±40% for the benzyl radicals. Turro's rough estimate of the diffusion-limited rate constant in *n*-hexane is $2 \times 10^{10}\ M^{-1}\ s^{-1}$.[42] However, the experimentally based value of Saltiel and Atwater for this same rate constant is $3.6 \times 10^{10}\ M^{-1}\ s^{-1}$.[41] The value of k_{BB} is half the value expected using the spin statistical factor of the reaction according to the value given by Saltiel and coincides with the expectations from the estimate of Turro.

For the ketone, $\phi_{BME\cdot,free} = 0.17 \pm 0.05$. Taking into account the fact that the dissociation of the ketone yields two BME· radicals, the primary dissociation quantum yield has a lower limit of 0.09 for this compound.

The above considerations demonstrate that whereas the ketone and the diazene yield very similar amounts of free BME· radicals in solution, this is a result of a compensation between a stoichiometrical factor favorable for the ketone and a higher primary dissociation yield for the diazene.

In conclusion, we have demonstrated that the diazene has very favorable features as a radical photoinitiator. It absorbs light at 365 and 254 nm, and in the latter band, an absorption coefficient of $2.05 \times 10^4\ M^{-1}\ cm^{-1}$ allows concentrations in the micromolar range to be used for photochemical applications. Because of the efficient internal conversion from the absorbing state to the dissociative state and photoisomerization being hindered by the appropriate substitution of the α carbons to the azo group, a high dissociation quantum yield is achieved ($\phi_{-diazene} = 0.50$). Finally, the diazene has also favorable kinetic behavior to make it a good probe for studying caging and clustering effects in supercritical fluids, which was one of our main aims in synthesizing this compound.

Acknowledgment. C.A.C. and P.F.A. are research staff from CONICET (Consejo Nacional de Investigaciones Científicas y Técnicas, Argentina). P.A.H., a Ph.D. fellow from CONICET, thanks DAAD (Deutscher Akademischer Austauschdienst) for a research grant. This work was performed under financial support from ANPCyT (PICT02 06-10621 and 06-33973) and UBA (X086).

Supporting Information Available: Complete experimental conditions. This material is available free of charge via the Internet at http://pubs.acs.org.

References and Notes

(1) Engel, P. S. *Chem. Rev.* **1980**, *80*, 99–150.
(2) Adam, W.; Oppenländer, T. *Angew. Chem., Int. Ed. Engl.* **1986**, *25*, 661–672.
(3) (a) Engel, P. S.; Ying, Y; He, S. *Macromolecules* **2003**, *36*, 3821–3825. (b) Rabek, J. F. *Mechanisms of Photophysical Processes and Photochemical Reactions in Polymers*; Wiley & Sons: New York, 1987.
(4) Diau, E. W.-G.; Abou-Zied, O. K.; Scala, A. A.; Zewail, A. H. *J. Am. Chem. Soc.* **1998**, *120*, 3245–3246.
(5) Diau, E. W. G.; Zewail, A. H. *ChemPhysChem* **2003**, *4*, 445–456.
(6) Fogel, L. D.; Steel, C. *J. Am. Chem. Soc.* **1976**, *98*, 4859–4867.
(7) Engel, P. S.; Wu, H.; Smith, W. B. *Org. Lett.* **2001**, *3*, 3145–3148.
(8) Boate, D. R.; Scaiano, J. C. *Tetrahedron Lett.* **1989**, *30*, 4633–4636.
(9) Scott, T. W.; Doubleday, C., Jr. *Chem. Phys. Lett.* **1991**, *178*, 9–18.
(10) Engel, P. S.; Steel, C. *Acc. Chem. Res.* **1973**, *6*, 275–281.
(11) Gould, I. R.; Zimmt, M. B.; Turro, N. J.; Baretz, B. H.; Lehr, G. F. *J. Am. Chem. Soc.* **1985**, *107*, 4607–4612.
(12) Chesta, C. A.; Mohanty, J.; Nau, W. M.; Bhattacharjee, U.; Weiss, R. G. *J. Am. Chem. Soc.* **2007**, *129*, 5012–5022.
(13) Kleinman, M. H.; Shevchenko, T.; Bohne, C. *Photochem. Photobiol.* **1998**, *67*, 198–205.
(14) O'Shea, K. E.; Combes, J. R.; Fox, M. A.; Johnston, J. P. *Photochem. Photobiol.* **1991**, *54*, 571–576.
(15) Turro, N. J.; Cheng, C. C.; Lei, X. G.; Flanigen, E. M. *J. Am. Chem. Soc.* **1985**, *107*, 3739–3741.
(16) Ramamurthy, V.; Corbin, D. R.; Turro, N. J.; Zhang, Z.; Garcia-Garibay, M. A. *J. Org. Chem.* **1991**, *56*, 255–261.

(17) By asymmetrically substituted compound, when applied to diazenes or ketones, we mean here a diazene or carbonyl group bound to two different groups on either side, yielding two different free alkyl radicals by photolysis.
(18) Hoijemberg, P. A.; Zerbs, J.; Japas, M. L.; Chesta, C. A.; Schroeder, J.; Aramendía, P. F. Photolysis of an asymmetrically substituted diazene in supercritical fluids and compressed gases: a cage effect study. *J. Phys. Chem. A*, in press.
(19) Hoijemberg, P. A.; Karlen, S.; Sanramé, C. N.; Aramendía, P. F.; García-Garibay, M. A. *Photochem. Photobiol. Sci.*, published online March 30, http://dx.doi.org/10.1039/b902272d.
(20) Bhandari, S.; Ray, S. *Synth. Commun.* **1998**, *28*, 765–771.
(21) Bertolotti, S. G.; Previtali, C. M. *J. Photochem. Photobiol., A* **1997**, *103*, 115–119.
(22) Carmichael, I.; Hug, G. L. *J. Phys. Chem. Ref. Data* **1986**, *15*, 1–250.
(23) Grimm, C.; Kling, M.; Schroeder, J.; Troe, J.; Zerbs, J. *Israel J. Chem.* **2003**, *43*, 305–317.
(24) Kaindl, R. A.; Wurm, M.; Reimann, K.; Hamm, P.; Weiner, A. M.; Woerner, M. *J. Opt. Soc. Am. B* **2000**, *17*, 2086–2094.
(25) Hamm, P.; Kaindl, R. A.; Stenger, J. *Opt. Lett.* **2000**, *25*, 1798–1800.
(26) Bergamini, G.; Ceroni, P.; Balzani, V.; Villavieja, M. d. M.; Kandre, R.; Zhun, I.; Lukin, O. *ChemPhysChem.* **2006**, *7*, 1980–1984.
(27) Chatgilialoglu, C.; Ingold, K. U.; Lusztyk, J.; Nazran, A. S.; Scaiano, J. C. *Organometallics* **1983**, *2*, 1332–1335.
(28) Rigorously, the rate of consumption of BME• radicals in Scheme 1 is

$$\frac{-\mathrm{d[BME]}}{\mathrm{d}t} = 2.k_{\mathrm{BB}}.(1-f_{\mathrm{esc}}).\,[\mathrm{BME}]^2 + k_{\mathrm{AB}}.(1-f'_{\mathrm{esc}}).[t-\mathrm{Bu}].[\mathrm{BME}] \tag{3}$$

From this rate expression, the definition of a second-order rate constant, $k_{2\mathrm{comb}}$, results in

$$k_{2\mathrm{comb}} = -\frac{1}{[\mathrm{BME}]^2}\frac{\mathrm{d[BME]}}{\mathrm{d}t} = 2.k_{\mathrm{BB}}.(1-f_{\mathrm{esc}}) + k_{\mathrm{AB}}.(1-f'_{\mathrm{esc}}).\frac{[t-\mathrm{Bu}]}{[\mathrm{BME}]}. \tag{4}$$

If we make the assumption that rate constants for the radical reactions and cage factors for the different radical encounters are all equal, then the concentrations of the two radicals are equal, and we arrive at the expression given in the text.

(29) Bensasson, R.; Land, E. J. *Trans. Faraday Soc.* **1971**, *67*, 1904–1915.
(30) Bensasson, R.; Amand, B. *Chem. Phys. Lett.* **1975**, *34*, 44–48.
(31) Kato, C.; Hamaguchi, H.-O.; Tasumi, M. *Chem. Phys. Lett.* **1985**, *120*, 183–187.
(32) Scott, T. W.; Liu, S. N. *J. Phys. Chem.* **1989**, *93*, 1393–1396.
(33) Srivastava, S.; Yourd, E.; E.; Toscano, J. P. *J. Am. Chem. Soc.* **1998**, *120*, 6173–6174.
(34) Tahara, T.; Hamaguchi, H.; Tasumi, M. *J. Phys. Chem.* **1987**, *91*, 5875–5880.
(35) Langkilde, F. W.; Bajdor, K.; Wilbrandt, R. *Chem. Phys. Lett.* **1992**, *193*, 169–175.
(36) Silva, C. R.; Reilly, J. P. *J. Phys. Chem.* **1996**, *100*, 17111–17123.
(37) Adam, W.; Trofimov, A. V. *Acc. Chem. Res.* **2003**, *36*, 571–579.
(38) We assume that there is no difference in the photochemistry of the diazene between 254 nm excitation (steady-state experiments where $f_{-\mathrm{diazene}}$ was determined) and 266 nm excitation (nanosecond pulses used to obtain the data in Figure 4).
(39) Shida, T. *Electronic Absorption Spectra of Radical Ions*; Elsevier: Amsterdam, 1988.
(40) Claridge, R. F. C.; Fischer, H. *J. Phys. Chem.* **1983**, *87*, 1960–1967.
(41) Saltiel, J.; Atwater, B. W. *Adv. Photochem.* **1988**, *14*, 1–90.
(42) Turro, N. J. Chapter 9. In *Modern Molecular Photochemistry*; University Science Books: Mill Valley, CA, 1991; p 314.

JP809315U